RESEARCH ARTICLE | FEBRUARY 22 1995

UV photostimulated desorption of ammonia from Cu(111)

T. Hertel; M. Wolf; G. Ertl

J. Chem. Phys. 102, 3414–3430 (1995)
https://doi.org/10.1063/1.469215

UV photostimulated desorption of ammonia from Cu(111)

T. Hertel, M. Wolf, and G. Ertl
Fritz-Haber-Institut der Max-Planck-Gesellschaft, Faradayweg 4-6, D-14195 Berlin, Germany

(Received 19 September 1994; accepted 14 November 1994)

Upon irradiation with 193 and 308 nm laser light photoinduced desorption of ammonia from Cu(111) was studied at three coverages less than one monolayer (ML). The linear power dependence of the desorption yield and angle-resolved translational energy distributions of desorbed molecules indicate that desorption occurs due to an electronic excitation rather than a thermal process. Polarization measurements indicate an excitation process which is mediated by hot substrate electrons. The isotope effect, i.e., the ratio of the cross sections for photostimulated desorption (at 193 nm) of NH_3 and ND_3, respectively, decreases from 4.1 ± 1.2 to 1.9 ± 0.5 when the coverage—with respect to the substrate atom density—was raised from $\approx$0.02 to $\approx$0.14 ML. The magnitude of this isotope effect suggests that the energy which is required to break the molecule–surface bond is acquired in an intramolecular coordinate during a short-lived electronic excitation. We propose that for high vibrational excitation on the ground-state potential energy surface (PES), efficient *coupling* of the inversion mode with the molecule–surface coordinate leads to desorption. In order to illustrate the suggested desorption mechanism at a semiquantitative level, we performed trajectory calculations on a two-dimensional model potential energy surface. The results predict that desorption occurs *rapidly* within a few vibrational periods of the umbrella mode ($T_{vib} \sim 35$ fs)—with comparable energy release into the translational and vibrational degrees of freedom. Ammonia is furthermore expected to desorb in an inverted geometry, i.e., with the hydrogen atoms pointing towards the surface as opposed to the adsorption geometry with the nitrogen end bound to the surface. Angular distributions of flux and mean translational energy are strongly peaked around the surface normal. Their width can be attributed to thermal motions parallel to the surface prior to excitation.

I. INTRODUCTION

Much of the current interest in the young field of surface photochemistry involving adsorbates is driven by the desire to unravel the microscopic events leading to photodesorption, photodissociation, and photoreaction.[1] State-resolved detection of products and isotopic substitution of photoexcited adsorbates may be used as powerful tools to gain new insights into the dynamics governing these processes.[2]

In contrast to the gas phase, little is known about excited electronic states of molecules at surfaces which play a key role in many photostimulated processes and also in chemical bonding at surfaces. [Throughout this article the term excited state will refer to *both* electronic excitation of the neutral molecule as well as formation of a temporary negative ion (or resonance). Although a resonance is not always associated with an excitation we use the term excited state in the sense that both processes result in a *temporary* change of the PES which governs the desorption dynamics.] Both the energetic location and lifetimes are expected to be significantly altered compared to gas phase due to interaction with the surface. Molecular resonances at metal surfaces, e.g., are frequently stabilized by interaction with the image potential.[3] On the other hand, lifetimes of excited states are assumed to be much shorter than in the gas phase, namely on the order of 10^{-15}–10^{-14} s due to new decay channels that are opened by the presence of a substrate.[4] Modeling of photostimulated surface processes may elucidate some of the changes which are introduced to molecules upon adsorption.

Desorption of ammonia by excitation with light or electrons has been investigated by a number of groups in the past decade. Photostimulated desorption of ammonia was first observed with infrared excitation of NH_3 or ND_3 adsorbed on Cu(100) by Hussla *et al.*[5] For NH_3 the authors found a resonant desorption cross section centered at the ν_1 asymmetric stretch around 3337 cm^{-1}. For coadsorption of NH_3 and ND_3 photodesorption of both species was observed at the same laser wavelength, i.e., isotopic selectivity due to resonant excitation was removed. The desorption mechanism was proposed to be a thermal process termed ''resonant heating'' where the asymmetric stretching mode of ammonia serves as an ''antenna'' for energy transfer from the incident radiation to molecular vibration. Coupling of the vibrational modes to the substrate phonon bath eventually leads to thermal desorption of the adsorbate.

In contrast to the resonant heating mechanism responsible for infrared laser-induced desorption, UV photostimulated desorption of ammonia and deuterated ammonia from GaAs(100)[6–8] was interpreted in terms of a modification of the frequently used Menzel–Gomer–Redhead[9,10] (MGR model) desorption scheme. The MGR model assumes that after an initial Franck–Condon transition from the ground to an excited-state potential energy surface, momentum, and, hence, kinetic energy is acquired by the nuclei due to the different equilibrium geometries in the two states. Fast deexcitation, within 10^{-15} to 10^{-14} s, returns the molecule to the ground-state potential energy surface while kinetic energy is conserved. The kinetic energy gained in this process can lead to desorption or dissociation. Naturally the amount of kinetic energy which is acquired during the lifetime on the excited-

 0021-9606/95/102(8)/3414/17/$6.00

state potential energy surface strongly depends on the nuclear mass for motion along the corresponding coordinate. A larger mass will lead to less acceleration and thus less kinetic energy is gained. As a consequence isotopic substitution may now help to identify the reaction coordinate responsible for energy transfer from electronic excitation to nuclear motion. In the ammonia/GaAs system the large isotope effect in the photodesorption cross sections of NH_3 and ND_3 of about 4 suggested that kinetic energy is acquired by an intramolecular coordinate during the excitation–deexcitation cycle. Zhu *et al.* first suggested that vibrational–translational energy transfer from an internal vibrational mode to the molecule–surface coordinate via coupling between both coordinates leads to desorption.[6,8,11] Therefore, the authors used the term vibrationally mediated photodesorption (VMPD) to describe the process.

A somewhat different desorption mechanism—which also employs a temporary electronic excitation as an intermediate to desorption—was proposed by Burns *et al.* for electron stimulated desorption of ammonia from Pt(111).[12,13] The authors observed a similar isotope effect ($\sigma_{NH_3}/\sigma_{ND_3} \approx 3$) and slightly higher mean translational energies compared to the NH_3/GaAs system. The authors suggest that a full inversion of the umbrella mode (time scale ~17 fs) in the excited state is required in order to induce desorption from a repulsive hard wall on the ground-state PES. The possibility of vibrational–translational ($V-T$) energy transfer was claimed to be unlikely. This seems plausible in view of the large frequency mismatch between intramolecular and the molecule–surface vibration and because of the short vibrational lifetime assigned to electronic damping on metal surfaces.[14,15] Molecular beam investigations by Kay *et al.*,[16] however, revealed significant translational–vibrational energy transfer when ammonia was scattered from a gold surface. We believe that the coupling observed by Kay *et al.* should also be operative for chemisorbed ammonia molecules which are vibrationally excited after quenching of an electronic excitation since the scattering experiments probe the same regions of the ground-state PES some 10 meV above the desorption threshold. Regardless of the differences in the two desorption schemes, the large isotope effect observed was attributed in both cases to nuclear motion along an *internal* molecular coordinate during the short-lived electronic excitation.

Photodesorption of ammonia was also studied for the NH_3/Ni and NH_3/NiO systems in an attempt to discern the role of the substrate in the excitation process.[17] Isotope effects, however, were not investigated.

In this article, we report on the results of a UV photodesorption study of ammonia from Cu(111) at three different adsorbate coverages in the submonolayer regime. At low coverage we find an isotope effect of 4.1 for photostimulated desorption of NH_3 and ND_3, respectively, which decreases to 1.9 with increasing coverage. The magnitude of the isotope effect suggests that nuclear motion along an internal ammonia coordinate in the excited state facilitates desorption as opposed to motion of the whole molecule with respect to the surface plane. The observed decrease in the isotope effect with increasing adsorbate coverage is in agreement with expectations from the standard Menzel–Gomer–Redhead (MGR)-type desorption process. Within the MGR model the desorption cross sections and thereby the isotope effect is determined by the desorption probability, i.e., the probability that an initial excitation leads to desorption. The coverage dependence of the isotope effect reported in this paper may basically be attributed to a variation of the desorption probability due to changes in the adsorbate binding energy.

As mentioned above, the magnitude of the isotope effect in stimulated desorption of ammonia was attributed to motion along an internal coordinate during a short-lived electronic excitation in all studies.[6,12,13] However, the mechanism by which energy could be transferred from molecular vibration to molecular motion remained rather unclear in the original articles by Zhu *et al.*[6] In this article we introduce—in contrast to the mechanism proposed by Burns *et al.*—a desorption mechanism which involves substantial energy interchange on the *ground-state* PES from the highly excited inversion mode of ammonia to the molecule–surface coordinate. Surprisingly, it turned out that the photodesorption cross sections for the ammonia/GaAs and ammonia/Cu(111) systems are rather similar. Naively this would not be expected if molecular vibrations were involved in the desorption process. The lifetime of the CO-substrate vibration, e.g., is known to decrease significantly from ~4 ms to ~2 ps when CO is adsorbed on an insulator[18] or metal[15] surface, respectively. The proposed coupling mechanism, however, will lead to *rapid* desorption within a few vibrational periods of the inversion mode so the vibrational lifetime is long with respect to the desorption process itself and vibrational damping plays only a minor role. To illustrate the proposed coupling mechanism we also report trajectory calculations on a model potential energy surface. The results of this calculation are discussed in view of the measured isotope effects, translational energy distributions, and the existing state-resolved studies of Burns *et al.*[12]

In addition to the coverage dependence of cross sections and translational energy distributions we report on the information that can be gained from angular distributions of photodesorbed molecules. The observed width of flux and mean translational energy distributions can be explained on the basis of a simple model and is attributed to thermal motions parallel to the surface prior to excitation. This suggests that during the desorption process translational energy is released essentially along the surface normal—a fact that reduces some of the complexity involved in the study of such a multidimensional system.

II. EXPERIMENT

Experiments were performed in an ultrahigh vacuum chamber, schematically depicted in Fig. 1. It was pumped by turbomolecular, Ti sublimation, and cryo pumps to reach a base pressure of $< 1 \times 10^{-10}$ mbar. The chamber was equipped with facilities for combined low-energy electron diffraction (LEED) and Auger electron spectroscopy (AES), thermal desorption measurements (TDS), photodesorbate time-of-flight (TOF), and electron time-of-flight spectroscopy.

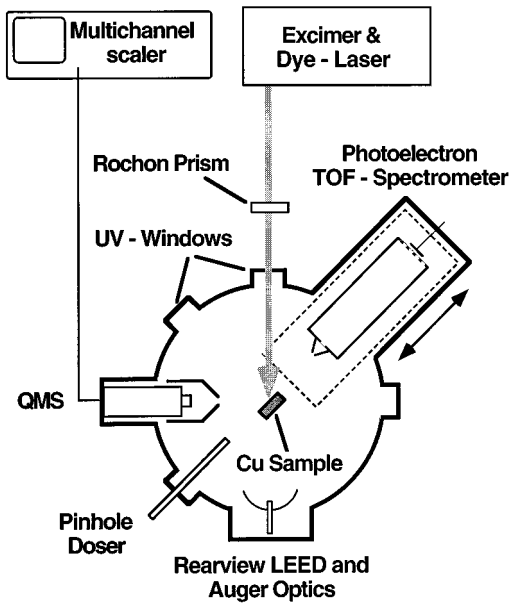

FIG. 1. Schematic drawing of the experimental apparatus.

The manipulator with differentially pumped rotational feedthrough provided *xyz* manipulation as well as rotation along the vertical axis. The Cu crystal was mounted between a pair of tantalum wires which were connected to a copper rod in thermal contact with a liquid-nitrogen-cooled reservoir. This allowed us to cool the crystal down to 85 K. The sample could be heated either by electron bombardment from a tungsten filament behind the crystal or resistively through the Ta wires. Sample preparation in ultrahigh vacuum was achieved by repeated cycles of soft (700 eV) Ar^+ sputtering at room temperature and successive annealing at 770 K. Surface cleanliness was checked by AES and by visual inspection of the quality of the LEED pattern.

NH_3 gas from Messer Griesheim had a stated purity of 99.997% and deuterated ammonia (ND_3) of 99.0% purity was obtained from Cambridge Isotope Laboratories (CIL). The sample was exposed to NH_3 or ND_3 through a pinhole doser with a 10 μm orifice. This allowed us to keep the background pressure as low as 2×10^{-10} mbar during exposure at a typical flux on the sample of $\approx$2 ML/min. The pressure in the reservoir attached to the doser was monitored by a capacitance manometer. Before experiments with ND_3 were performed, the doser was passivated with several fillings of ND_3 gas for at least one day to avoid isotopic substitution on the walls of the reservoir. The isotopic purity of the sample (ND_3:ND_2H:NDH_2:NH_3) was estimated from TOF measurements of photodesorbed ammonia and from thermal desorption data. From these experiments we estimated the isotopic purity of ND_3 on the surface to be better than 90%. Note that isotopic substitution on the chamber walls prior to detection may prevent reliable estimates on isotopic composition on the sample. For coadsorption of both isotopes, ND_3 was dosed from the pinhole while NH_3 was provided from a leak valve in order to avoid isotopic mixing in the reservoir.

The relative ammonia coverages after adsorption and subsequent laser-induced desorption were monitored by integration of thermal desorption spectra. The desired ammonia coverages were obtained by maintaining the sample at a certain temperature and saturating it with the appropriate amount of ammonia. Saturation of the sample was ensured by investigation of the uptake as a function of time at the three adsorption temperatures. For coadsorption of NH_3 and ND_3 we reached the desired coverages directly by offering appropriate amounts of gas. This, however, leads to somewhat less reproducible coverages.

For irradiation of the sample with light at 193 nm we employed an excimer laser (Lambda Physik, EMG 150 MSC) filled with an ArF mixture, while for measurements at 308 nm we used a second excimer laser (EMG 200E) operating with a XeCl mixture. Unless otherwise mentioned, the laser-induced desorption measurements were performed at a sample temperature of 85 K. For all experiments care was taken to ensure uniform illumination of the whole sample by use of a telescope. The resulting beam profile was controlled by visual inspection of the burn pattern produced by the laser beam on photosensitive paper. The pulse fluence was reduced to less than 10 mJ/cm^2 (typical 5 mJ/cm^2). Based on the equations given by Burgess *et al.*[19] and the optical data given in Ref. 20, the transient temperature rise of the irradiated sample surface for this fluence should be less than 35 K. The possibility of laser-induced thermal desorption could also be ruled out from the linear power dependence of the desorption yield (see below). Polarization of the unpolarized laser light was achieved by use of a Rochon prism directly in front of the UV windows at the chamber.

The quadrupole mass spectrometer (Balzers, QMS 112A), equipped with a cross-beam ion source, viewed the crystal with an angular resolution of $\pm 4°$ and can be considered to be a well collimated detector. To reduce diffuse background in photodesorption TOF measurements a copper shield surrounding the ion source and part of the spectrometer was cooled with liquid nitrogen. Photodesorption TOF spectra were recorded with a multichannel scaler (SRS 430) following pulsed laser irradiation of the Cu surface as described below. The ionizer-sample distance was 62 mm and the NH_3 ion flight time through the quadrupole was estimated to be 14 ms. Relative NH_3/ND_3 desorption signals were obtained assuming the same ionization cross sections for both isotopes.

The procedure for the quantitative analysis of the TOF spectra has been described elsewhere.[21] The analysis has to take into account that mass spectroscopic detection measures the particle density. The mean translational energy $\langle E_{\text{trans}} \rangle$, the mean velocity $\langle v \rangle$, and the variance $\langle \sigma^2 \rangle$ can be derived by numerical integration from the flux-weighted curves.

Angular distributions of photodesorbed molecules were obtained from integration of flux-weighted TOF spectra. The angle between the incoming light and detected desorbates was either 45° or 90° due to the fixed positions of the QMS and our two UV windows. The measured flux at different sample orientations was thus normalized to the incident laser fluence per unit area normal to the crystal surface. To account for the decrease in the desorption yield due to a decrease in adsorbate coverage during data acquisition, the flux

was also corrected using the previously determined photodesorption cross sections.

The 6.4 and 3.5–4.0 eV output of the excimer or dye laser was also used to record one- and two-photon photoemission spectra. Kinetic energy distributions of photoemitted electrons were obtained by the time-of-flight technique. For these measurements the sample was positioned inside a retractable electron TOF spectrometer shielded with a cylinder of high-permeability alloy. The field-free flight region inside a gold coated tube was 30 cm in length and the estimated collection angle of the detector was $\pm 3.5°$. Electrons leaving the field-free region were accelerated and focused onto a fast channeltron. A photodiode signal from the laser pulse served as a time reference and flight times were recorded with a multichannel scaler allowing 5 ns time resolution. The overall time resolution, however, was limited by the length of the laser pulses ranging from 13 to 25 ns.

The performance of the spectrometer for one- and two-photon photoemission has been tested using the well-known Shockley state of the Cu(111) surface located 0.4 eV below the Fermi level.[22] The energy resolution for direct photoemission (1PPE) with $h\nu = 6.4$ eV at ≈ 1 eV kinetic energy was determined to be 150 meV while for two-photon photoemission (2PPE) at ≈ 2.5 eV kinetic energy it was 250 meV. In order to avoid space charge broadening, the pulse fluence for 1PPE was kept below 5 nJ/cm^2 while for 2PPE it was kept below ≈ 5 mJ/cm^2. The absolute work function was determined from the width of the 1PPE or 2PPE spectra. The change in the work function at different ammonia coverages was determined from the secondary electron cutoff which could be measured with a precision of ≈ 50 meV. For the clean surface the work function was found to be 4.85 ± 0.10 eV in good agreement with results reported elsewhere.[23,24]

III. RESULTS

To the best of our knowledge the ammonia–Cu(111) system has not yet been investigated with TDS or work function measurements. Therefore, we will first characterize the system using our thermal desorption and work function data before we proceed with the results of the photostimulated desorption. These will include the coverage dependence of cross sections and isotope effects as well as translational-energy and flux angular distributions of desorbed ammonia.

A. Thermal desorption data and work function measurements

A series of mass 17 thermal desorption spectra following adsorption of different amounts of NH_3 at 85 K is reproduced in Fig. 2. The heating rate was ≈ 8 K/s. With increasing coverage, desorption features labeled α, β_1, β_2 and the multilayerlike desorption feature γ develop. In order to obtain rough estimates for the binding energies at the respective α, β_1, and β_2 coverages we used Redhead's peak maximum method assuming first-order desorption kinetics and a frequency factor of 10^{13} s^{-1}. An evaluation of desorption temperatures then yields activation energies for desorption at the α coverage ($T_{max} = 275$ K) of ≈ 0.71 eV, at the β_1 coverage ($T_{max} = 190$ K) an activation energy of ≈ 0.48 eV, and at the β_2 coverage ($T_{max} = 140$ K) an activation energy of ≈ 0.35 eV. These numbers should be considered with caution since Redhead's peak maximum formula is strictly applicable only for coverage independent binding energies. For the adsorption of ammonia on metal surfaces this is certainly not the case due to the strong permanent dipole moment of ammonia (1.47 D) leading to coverage dependent repulsive interactions. Probably more reliable values for the activation energy to desorption at very small ammonia coverages [$\theta \ll 1$ monolayer (ML)] were obtained by Wu and Kevan for the ammonia/Cu(100) system.[25] By means of isothermal desorption measurements these authors derived an activation energy of 13.6 kcal/mol for NH_3 (0.59 eV) and 14.7 kcal/mol for ND_3 (0.64 eV). Since the thermal desorption traces appear to be similar for both the Cu(100) and Cu(111) surfaces,[5] we assume that this method provides more accurate values for the activation energy at low coverage also for the ammonia/Cu(111) system than the crude estimate from the position of thermal desorption maxima. The surprising difference in binding energies for isotopically labeled ammonia may tentatively be attributed to different zero point energies of the frustrated molecular motions but transition state theory was used to fully account for the effect.[25]

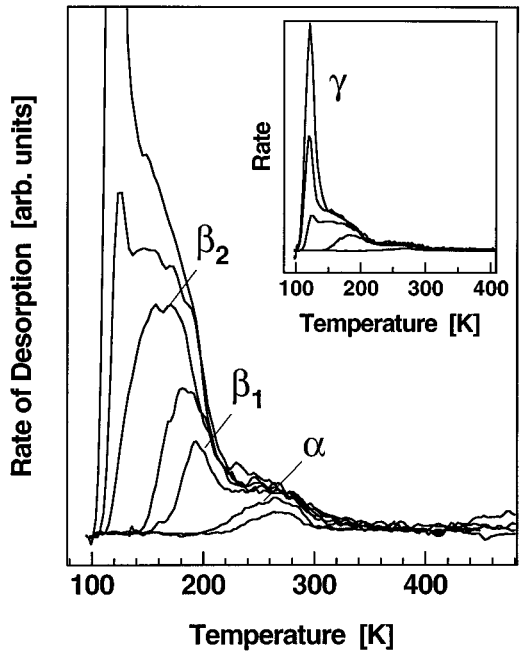

FIG. 2. Thermal desorption spectra of NH_3 (mass 17 u) after adsorption of different amounts of ammonia at 85 K. The heating rate was ≈ 8 K/s. From our work function measurements the β_2 coverage is estimated between $\theta = 0.12$ to 0.16 monolayer (ML) with respect to the substrate atom density of Cu(111). The inset shows the growth of the desorption feature γ with increasing ammonia exposure.

With increased exposure, the onset of the desorption feature γ starts to overlap with desorption from the β_2 feature. For photodesorption experiments the desired coverages were prepared by saturation of the surface with an exposure equivalent to a few monolayers at 120 (β_2 coverage), 170 (β_1 coverage), or 230 K (α coverage), respectively. These were the only ammonia coverages investigated in the photodesorption experiments and in what follows we will refer to them

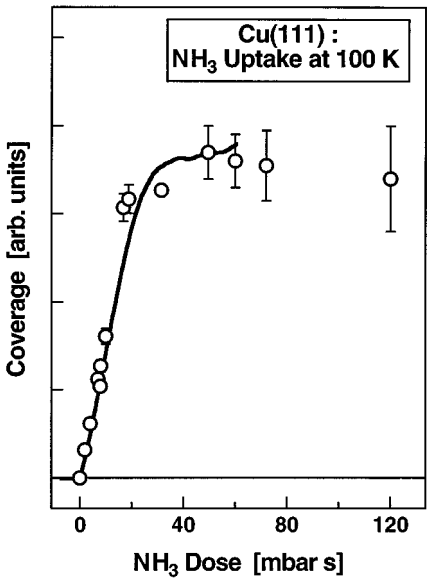

FIG. 3. Ammonia coverage vs NH_3 exposure expressed in mbar s at an adsorption temperature of 100 K. The dose refers to the integral of the pressure in the reservoir of the pinhole doser over time. This should not be confused with the ammonia partial pressure at the crystal which is not known. The open markers indicate ammonia coverages derived from thermal desorption spectra while the solid line was obtained from integration of the ammonia partial pressure during exposure (see the text).

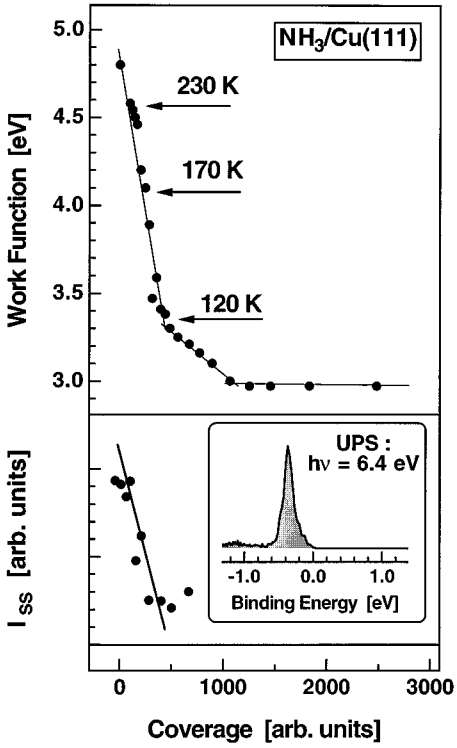

FIG. 4. Upper panel: work function vs NH_3 coverage as obtained from the width of photoelectron spectra. The work function at the three investigated coverages α, β_1, and β_2 is indicated by arrows and the corresponding adsorption temperatures (230, 170, and 120 K for the α, β_1, and β_2 coverages, respectively). Lower panel: intensity of the Cu(111) surface state vs coverage ($h\nu=6.4$ eV). The inset shows a typical photoelectron spectrum from which the intensity of the surface state was derived.

using the Greek letters. In order to ensure that no multilayer adsorption occurs at the chosen ammonia flux and at all adsorption temperatures we measured the ammonia uptake as a function of exposure. For an adsorption sample temperature of 100 K, the results of this experiment, as derived from integration of thermal desorption traces recorded immediately after exposure, are depicted in Fig. 3. An alternative method to monitor the ammonia uptake is to record the ammonia partial pressure (above the mass 17 background signal) during exposure. It should be proportional to the fraction r of impinging molecules not adsorbed by the surface. Integration of the sticking probability $S \propto (1-r)$ over time should then yield the desired uptake to within a proportionality constant. In Fig. 3 we, therefore, also plotted the uptake derived from integration of the ammonia partial pressure during exposure (solid line) which is in nice agreement with the results from the thermal desorption measurements. The observed linear increase in the accumulated coverage followed by saturation indicates that no multilayer adsorption occurs at an adsorption temperature as low as 100 K and consequently also not at all higher temperatures.

Coadsorption experiments of NH_3 and ND_3 in combination with photodesorption TOF measurements showed no sign of thermally induced isotopic mixing at the surface.

In order to obtain more accurate estimates for the absolute coverages we measured the decrease in the work function and surface state intensity with UPS ($h\nu=6.4$ eV) and two-photon photoemission (2PPE, $h\nu=3.55$ eV). The work function ϕ which was obtained from the width of the two-photon photoelectron spectra is depicted in Fig. 4 as a function of coverage; the latter being derived from integration of the corresponding thermal desorption traces. For the clean surface we obtained a value of $\phi=4.85 \pm 0.10$ eV. Clearly evident is the linear decrease down to $\phi=3.30$ eV which corresponds to a change of $\Delta\phi=-1.55$ eV. At saturation the work function has been lowered by 1.9 eV. This is in qualitative agreement with previous observations for ammonia adsorbed on Pt(111)[26] and Ru(0001),[27] e.g., where the work function change $\Delta\phi$ at saturation was -3.0 and -2.4 eV, respectively. Using the Helmholtz equation ($\Delta\phi = -4\pi e\mu n$, where e is the elementary charge, μ the dipole moment, and n the adsorbate density) we may now estimate the absolute coverages given that ammonia adsorbs in the expected geometry with the nitrogen end pointing towards the surface[28,29] and the molecular axis perpendicular to the surface plane. If we use the gas-phase dipole moment as a lower bound and the induced dipole moment for adsorption on transition metal surfaces[26,27] ($\approx$2 D) as upper bound for the ammonia/Cu system, we obtain an absolute coverage of 2.1×10^{14} to 2.8×10^{14} cm^2 at 120 K adsorption temperature. This corresponds to a coverage θ of 0.12 to 0.16 with respect to the substrate atom density at $T_{ads}=120$ K and a coverage $\theta=0.24$–0.32 at saturation of the work function. Assuming a similar adsorbate density at monolayer coverage as in the ammonia/Ru(0001) system ($\theta_{ML}\approx 0.25$), we may tentatively assign the saturation of the work function to completion of the first adsorbate layer in the ammonia/Cu(111) system. The leveling off in the work function curve

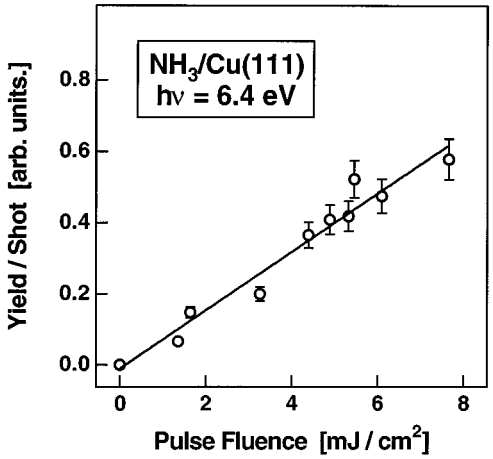

FIG. 5. Dependence of the ammonia desorption yield on laser pulse fluence at $h\nu = 6.4$ eV up to 8 mJ/cm^2. The linear increase indicates that desorption is not due to laser-induced heating of the surface.

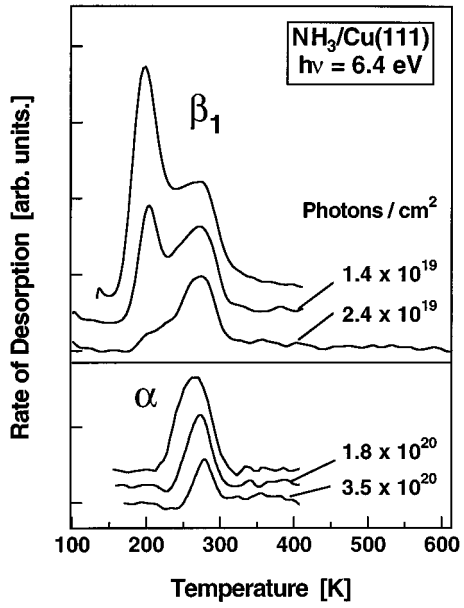

FIG. 6. Thermal desorption (TD) spectra taken before and after irradiation of the ammonia covered surface with 6.4 eV photons. Upper half: TD spectra after initial preparation of the β_1 coverage and irradiation with 0, 1.4, and 2.4×10^{19} photons/cm^2, respectively. Lower part: TD spectra after initial preparation of the α coverage and photon doses of 0, 1.8, and 3.5×10^{20} photons/cm^2.

at half the estimated monolayer coverage is likely to result from dipole–dipole interactions leading to neutral depolarization. We think it is safe to assume that ammonia molecules are not tilted at the coverages investigated (α,β_1,β_2), which all fall into the region of the initial linear decrease in the work function.

Using photoemission at 6.4 eV, we were also able to follow the evolution of the Cu(111) surface state with varying adsorbate coverage. The linear decrease in work function nicely correlates with the decrease in the surface state intensity which cannot be attributed to attenuation of the photoemitted electrons by the adsorbate layer, see Fig. 4. Obviously the surface state is completely quenched only at coverages beyond at least half a monolayer.

B. Photodesorption cross sections

The yield of photodesorbed ammonia was found to increase linearly with laser fluence up to at least 8 mJ/cm^2 ($h\nu = 6.4$ eV) as shown in Fig. 5. This indicates that desorption occurs due to an electronic rather than a thermal process for which a stronger than linear increase of the desorption yield is expected. Measurements of the relative desorption yield at masses 15, 16, and 17 (NH,NH_2,NH_3) from TOF spectra reproduced the ratios known from the ammonia QMS cracking pattern. TOF distributions were also identical for the different fragments. Thus within the limits of this analysis, the detected fragments are produced in the ion source from the desorbed ammonia parent and not by a stimulated surface process. This observation was further reinforced by the shape of post-irradiation TD spectra which showed no sign of recombinative thermal desorption of NH_2 and atomic hydrogen at higher desorption temperatures. From these results we estimated that the cross section for photon induced decomposition of NH_3 at the surface is smaller than 10^{-22} cm^2. In contrast, deuterated ammonia is dissociated upon irradiation on the GaAs(100) surface[7] with a cross section of $\approx 10^{-21}$ cm^2 at 6.4 eV.

The cross sections for photostimulated desorption are determined from the decrease of the adsorbate coverage with photon exposure. This decrease can be monitored by integration of post-irradiation TD spectra or, alternatively, from the decrease in the ammonia TOF signal during photon exposure. Especially at low adsorbate coverages, however, the TOF measurements may lead to systematic errors due to minority species with higher desorption cross sections or due to changes in the desorption dynamics with varying coverage, e.g., a change in the angular distribution of desorbing molecules. To avoid these problems for the two low coverage phases (α and β_1), we therefore determined the decrease in ammonia coverage Θ from integration of TD spectra taken after photon exposure. Starting at identical coverages this procedure was repeated for the α and β_1 phases for a number of different photon doses. In addition, the cross section for the β_1 phase was also determined from the decrease in the TOF signal. The cross sections for the high coverage phase β_2 were determined by the time-of-flight technique only. Assuming first-order desorption in coverage Θ and a linear power dependence, the differential cross section σ_{des} is then obtained from the slope of a $\ln(\Theta)$ vs exposure curve,

$$\sigma_{\mathrm{des}} = -\frac{d\,\ln(\Theta)}{df},$$

where f is the photon fluence.

A series of post-irradiation TD spectra is displayed in Fig. 6 [starting from the β_1 coverage (upper panel) and the α coverage (lower panel), respectively]. It can be seen that much higher photon doses are needed to remove an identical fraction of the coverage when starting with the low coverage

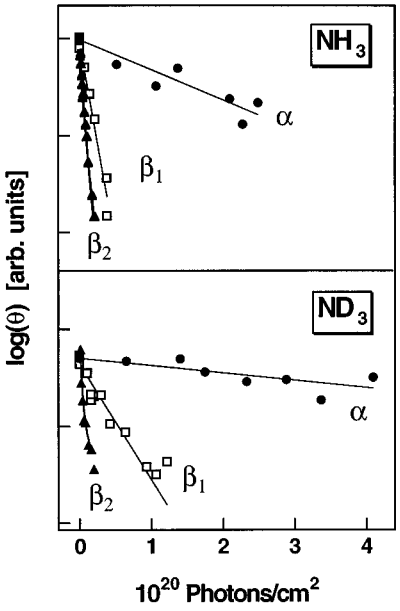

FIG. 7. Logarithm of the residual coverage (α and β_1 phase) after irradiation and logarithm of the photodesorption yield (β_2 phase) vs photon exposure ($h\nu=6.4$ eV). For the two smaller coverages the residual coverages were derived from integration of post-irradiation TD spectra in order to avoid systematic errors.

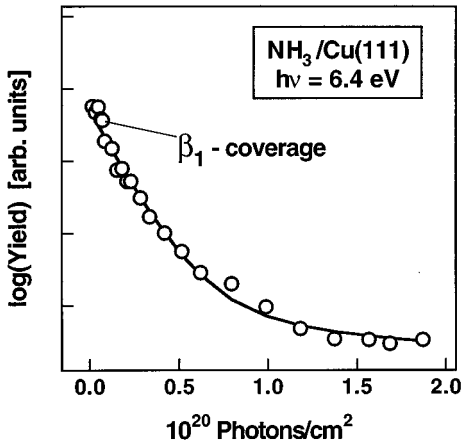

FIG. 8. Logarithm of the NH_3 photodesorption yield vs photon dose ($h\nu=6.4$ eV) as obtained from integration of TOF spectra after initial preparation of the β_2 coverage. The desorption cross section is derived from the initial slope. The decline of the slope reflects the continuously decreasing photodesorption cross section as the coverage is reduced. Within a simple Menzel–Gomer–Redhead-type desorption scheme this can be attributed to an increase in binding energy (when going to smaller coverages) giving rise to a reduced desorption probability.

α phase if compared with the higher coverage phase β_1. The α-peak position shifts to higher temperature with increasing photon exposure, i.e., decreasing adsorbate coverage. This closely follows the evolution of thermal desorption features as a function of coverage upon NH_3 adsorption.

Residual NH_3 and ND_3 coverages after photon exposure at normal incidence and 85 K are reproduced in Fig. 7 as a function of laser fluence. The resulting cross sections σ_{des} for desorption with 193 nm laser light (6.4 eV) are displayed in Table I together with the corresponding isotope effect (ratio of $\sigma_{\mathrm{NH_3}}/\sigma_{\mathrm{ND_3}}$). While the absolute cross section for photodesorption of NH_3 (at 193 nm) increases in going from the low to the high coverage phase by a factor of 30, the same cross sections for photodesorption of ND_3 increase by a factor of 65. This gives rise to the observed decrease in the isotope effect from 4.1 to 1.9 when the coverage is increased. The continuous decrease in the photodesorption cross sections is also evident from the variation of the slope in the semilogarithmic plot of yield vs photon exposure, see Fig. 8. Within the error bars of the analysis the cross sections as determined from post-irradiation thermal desorption spectra and from the time-of-flight experiments are identical.

TABLE I. Cross sections for photostimulated desorption of ammonia from Cu(111) at different adsorbate coverages and photon energies.

	α ($T_{\mathrm{ads}}=230$ K) ($10^{-20}\mathrm{cm}^2$)	β_1 ($T_{\mathrm{ads}}=170$ K) ($10^{-20}\mathrm{cm}^2$)	β_2($T_{\mathrm{ads}}=120$ K) ($10^{-20}\mathrm{cm}^2$)
Cross section NH_3			
6.4 eV	0.31	4.1	8.7
4.0 eV	···	0.18	0.84
Cross section ND_3			
6.4 eV	0.07	1.2	4.6
Isotope effect	4.1±1.2	3.4±1.3	1.9±0.5

From TOF experiments we also determined cross sections for photostimulated desorption at 308 nm ($h\nu=4.0$ eV), see Table I. The corresponding cross sections at the β_1 and β_2 coverages are about a factor 10 to 30 smaller than those measured at 193 nm. This observation is typical for a number of systems,[8,30,31] where the desorption cross sections are all found to increase more than linearly with photon energy.

When NH_3 and ND_3 were coadsorbed the isotope effect was not removed and we observed basically the same cross sections and isotope effects for irradiation with 193 nm laser light. This argues against intermolecular energy transfer between adsorbates and excludes the resonant heating mechanism for UV photodesorption which was proposed for infrared laser-induced desorption of ammonia from Cu(100) by Hussla *et al.*[5] As mentioned earlier these authors observed that the isotope effect resulting from resonant excitation of the asymmetric stretch was completely removed when NH_3 and ND_3 were coadsorbed.

C. Time-of-flight and angular distributions of photodesorbed ammonia

Time-of-flight distributions were measured at both wavelengths (193 and 308 nm) for detection along the surface normal. The velocity distributions reproduced in Fig. 9 where obtained from TOF distributions by conversion to the flux domain and using the Jacobian $dt \propto v^{-2}\, dv$. Fitting with a modified Maxwell–Boltzmann distribution[2] yields the values for the mean energy in the flux domain listed in Table II. Within the error bars the mean translational energies (at 193 nm excitation wavelength) are independent of coverage for both isotopes (102 ± 7 meV for NH_3 and 93 ± 9 meV for

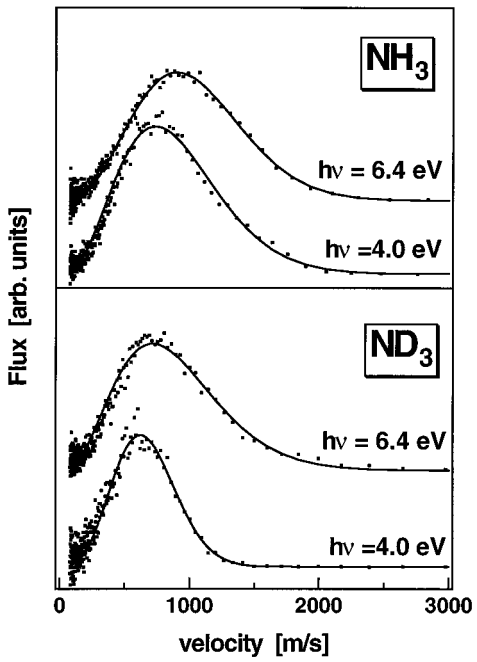

FIG. 9. The velocity distributions obtained from time-of-flight distributions ($h\nu=6.4$ and 4.0 eV, respectively) measured along the surface normal for the β_2 coverage of NH_3 (upper panel) and ND_3 (lower panel), respectively. The mean translational energies derived from these spectra are listed in Table II.

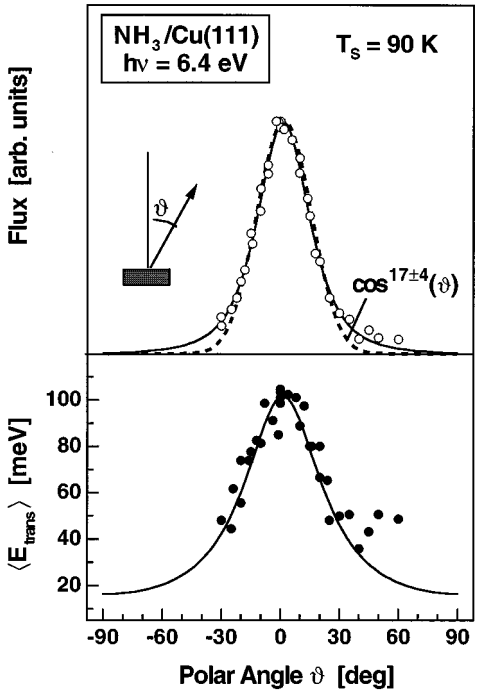

FIG. 10. Flux (upper panel) and mean translational energy (lower panel) of photodesorbed NH_3 ($h\nu=6.4$ eV) vs detection angle ϑ obtained at 90 K sample temperature. The detection angle ϑ is measured with respect to the surface normal (see inset). The flux distribution can be fitted with a $\cos^{17\pm4}(\vartheta)$ angular dependence (dashed line). The model described in the text yields an excellent fit to the angular dependence of both flux and mean translational energies (solid lines).

ND_3). Similarly to photostimulated desorption of ammonia from GaAs(100) and for electron stimulated desorption in the ammonia/Pt(111) system where no differences in the translational energies for both isotopes were reported, we observe that NH_3 and ND_3 desorb with nearly the same kinetic energy. The trends in our experimental data, however, suggest a slightly higher $\langle E_{\text{trans}}\rangle$ for NH_3 than for ND_3. When the excitation wavelength is changed from 193 (6.4 eV) to 308 nm (4.0 eV) the mean translational energies become significantly smaller. Evaluation of the time-of-flight spectra yields 87 ± 6 meV for NH_3 (β_1 and β_2 coverage only) and 52 ± 2 meV for ND_3 (β_2 coverage only). Again no significant coverage dependence is observed at this photon energy, however, the mean translational energy of photodesorbed ND_3 is clearly smaller than that of NH_3. Values for the variance $\langle\sigma^2\rangle$ obtained from the fitting procedure are all close to that corresponding to a thermal Maxwell–Boltzmann distribution (0.13). The observation that a decrease in photon energy is paralleled by a decrease in translational energy of photodesorbed molecules was also made for photostimulated desorption of O_2 from Pt(111).[31]

TABLE II. Mean translational energies, $\langle E_{\text{trans}}\rangle$, of ammonia photodesorbed from Cu(111) for different adsorbate coverages and photon energies. Errors are supposed to reflect the margins as given by the signal-to-noise ratio and the fit procedure. Additional systematic errors should not be relevant for a comparison of the values obtained at identical experimental conditions.

	α (T_{ads}=230 K)	β_1 (T_{ads}=170 K)	β_2 (T_{ads}=120 K)
NH_3: $\langle E_{\text{trans}}\rangle$			
6.4 eV (meV)	96±10	101±7	107±4
4.0 eV (meV)	···	90±5	84±8
ND_3: $\langle E_{\text{trans}}\rangle$			
6.4 eV (meV)	86±10	95±9	98±9
4.0 eV (meV)	···	···	52±2

The angular distributions of the NH_3 photodesorption yield as well as the corresponding mean translational energies are strongly peaked in the normal direction. In particular the latter effect is indicative for a photochemical rather than a thermal process. This was already suggested by the linear power dependence of the photodesorption yield. In Fig. 10 the angular distributions for the high coverage β_2 phase are reproduced for irradiation at a sample temperature T_s of 85 K. Fitting the data with a cosine law $[\cos^n(\vartheta)]$ yields best results for an exponent n of 17 ± 4. *A priori*, however, there is no physical justification for fitting with a $\cos^n$ distribution. We have, therefore, developed a simple model which accounts for the influence of thermal molecular motions parallel to the surface prior to excitation and the energy released along the surface normal. The angular distributions of both flux and mean translational energy can be fitted very well using the equations introduced in the discussion (see below). As seen in Fig. 10 the mean translational energies also show an angular dependence which is peaked in the normal direction and decreases from $\langle E_{\text{trans}}\rangle\approx105$ meV at $\vartheta=0°$ down to $\langle E_{\text{trans}}\rangle\approx35$ meV at $\vartheta=50°$. The angular distributions for the two low coverage phases (α and β_1) are the same as for the β_2 phase. However, they could not be measured with the same precision due to the reduced signal-to-noise ratio. No

influence of the substrate temperature on the translational energy distribution is observed for T_s ranging from 85 to 165 K (β_1 phase).

IV. DISCUSSION

The photostimulated desorption of ammonia at 193 and 308 nm is found to be the result of an electronic excitation rather than a thermal process. This becomes evident from the linear power dependence of the desorption yield as well as the small calculated temperature rise during the pulse duration[19,20] and the angular flux distributions which are strongly peaked around the surface normal. The results of our measurements, in particular the isotope effect, will give us some insight into the underlying mechanism that leads to photostimulated desorption. The following discussion will in principle follow the individual steps of the photodesorption process. Starting with the initial adsorbate excitation we will discuss what can be learned from the polarization dependence of the photodesorption yield (described below). The precise nature of the excited state is, unfortunately, not known but some of its fundamental characteristics can be guessed from what is known about excitation of gas-phase ammonia by interaction with either photons or electrons. We then discuss the isotope effect which is attributed to the perturbation of the internal equilibrium geometry of the molecule during the short-lived electronic excitation. The suggested desorption mechanism which involves energy transfer from the inversion mode to the molecule–surface coordinate after decay of the electronic excitation is also discussed in some detail. To illustrate the proposed coupling mechanism at a semiquantitative level we report on trajectory calculations on a model potential energy surface.

A. Excitation mechanism

Since the results of the photodesorption measurements at 193 and 308 nm indicate that ammonia is desorbed as a consequence of an electronic excitation, we have to elucidate how the incident photon energy is coupled into the adsorption complex. While the path for adsorbate excitation may be traced on the basis of the polarization dependence of the yield we can only speculate on the character of the excited state itself. Nonetheless, provided with the broad knowledge from excitations of gas-phase ammonia this speculation seems to be worthwhile since it yields valuable insights into the dynamics in the excited state of free and to some extent also for adsorbed ammonia. Theoretical calculations as well as experimental data on the adsorption geometry and vibrational excitation of ammonia on Cu(100), e.g., reveal that neither the intramolecular equilibrium geometry of free ammonia nor its vibrational modes are significantly altered upon adsorption.[25,32,33] Apart from this, the strength of the chemisorption bond is to some extent attributed to electrostatic interactions of the adsorbates dipole moment with the substrate electrons and not exclusively to covalent bonding.[28] This encourages us to assume that some of the main characteristics of gas-phase ammonia (and its excitations) survive in the presence of the surface.

When the surface is irradiated with light the adsorbate may either be excited directly by the electric field at the surface or indirectly by photogenerated electron-hole pairs. Luckily, discrimination of both processes is feasible if the transition dipole moment for optical excitations is perpendicular to the surface plane.[34] This can be achieved by investigation of the polarization dependence of the desorption cross section. This is due to the fact that a substrate mediated process will scale with the polarization dependence of light absorption in the bulk while the direct process will depend on the components of the electric field strengths in the surface region. The following evaluation of the polarization measurements based on Fresnel's equations has been reviewed elsewhere[35] and has been applied with success to a number of systems.[31,36,37] The components of the mean square electrical field strengths of the standing wave at the surface boundary and the absorption for s- and p-polarized light are reproduced in the upper panel of Fig. 11 as a function of the angle of incidence (measured with respect to the surface normal). They were computed from the equations given in Ref. 35 using the optical constants for Cu.[20] Here s-polarized (p-polarized) refers to light whose electric field vector lies perpendicular (parallel to) the plane of incidence as defined by the incoming and reflected beams. In order to reduce systematic errors from the different instrumental arrangement at different angles of incidence ϑ_i we measured the ratio of the desorption yield σ_p/σ_s rather than the absolute cross sections for each angle. The results are displayed together with the ratios A_p/A_s for light absorption by the

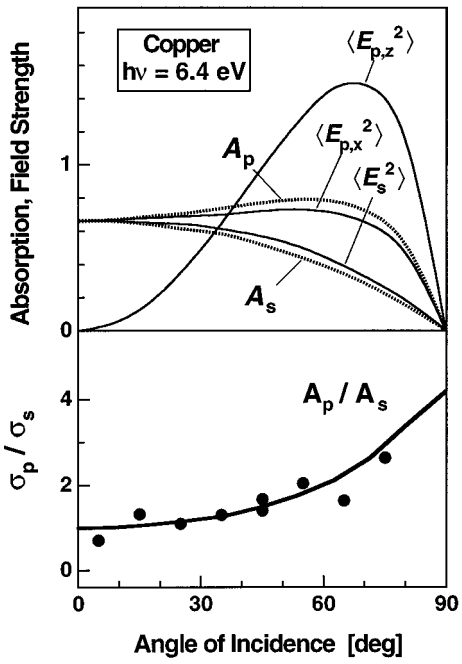

FIG. 11. Dependence of the calculated electrical field strengths and substrate absorption on polarization and angle of incidence for light impinging on a copper surface with $h\nu = 6.4$ eV (upper panel). The subscripts p and s refer to light polarized with the electric field vector parallel or perpendicular to the plane of incidence, respectively. For p polarization the components normal (parallel) to the surface are indicated by $z(x)$. Lower panel: ratio of the NH_3 desorption yield σ_p/σ_s for p and s polarized light (solid circles) and ratio of the corresponding substrate absorption A_p/A_s. The results indicate a substrate mediated excitation process (see text).

bulk in the lower panel of Fig. 11. The good agreement between the experimental ratios and those obtained from bulk absorption strongly suggests that the process is substrate mediated. However, in order to exclude a direct excitation mechanism we also have to compare this to the ratios expected for such a direct process. Therefore, we have to know which components of the electric field $\langle E_{p,x}^2 \rangle$, $\langle E_{p,z}^2 \rangle$, or $\langle E_s^2 \rangle$ are required to excite the molecule. For this purpose let us briefly review what is known about optical excitations of gas-phase ammonia.

It is now generally accepted that all known excited electronic states $\tilde{A}$, $\tilde{B}$, $\tilde{C}$, etc. of gas-phase ammonia are Rydberg in character.[38] Each of the identified electronic excitations involves promotion of one $3a_1$ lone pair electron which is accompanied by a transition from the pyramidal (C_{3v} symmetry) ground state to a planar (D_{3h} symmetry) configuration in the excited state. This change in symmetry implies that the molecule can be excited only by electric field components parallel to the molecular symmetry axis. For ammonia adsorbed on Cu(111), the molecular axis is believed to be perpendicular to the surface plane (see above). The probability distribution of the molecular orientation due to frustrated rotations can be safely neglected since it would have a Gaussian width of less than 9° [estimated from the excitation energy for the frustrated rotation ρ_r for NH_3 on Cu(100)[33] of 560 cm^{-1}]. For simplicity let us now assume that the orientation (with respect to the molecular symmetry axis) of the transition dipole moment for optical excitations of adsorbed ammonia is not altered substantially with respect to the gas phase. The expected molecular orientation to the surface plane would thus require that the adsorbed ammonia can practically only be excited by the z component $\langle E_{p,z}^2 \rangle$ of the incoming laser light. Thus one would expect that the ratio of the desorption yield for p- and s-polarized light would increase tremendously ($\sigma_p/\sigma_s \gg 1$) at higher angles of incidence which is clearly not the case.

From these considerations we conclude that light absorption in the metal, which leads to production of electron-hole pairs, constitutes the first and predominant step in the investigated desorption process. In principle the excitation may then proceed by electron scattering from or attachment to the adsorbate or similar interactions including a hole. The mobility of holes, however, is in general assumed to be much lower than that of electrons which leads to a greatly reduced scattering frequency in the surface region. Adsorbate excitation via electron scattering thus seems more likely.

In this context it is noteworthy that for resonant electron scattering by gas-phase NH_3 and ND_3 Arfa *et al.* have observed isotope effects ranging from 1.36 to 2.50 (depending on the vibrational level that was excited) for the asymmetric stretching mode $\nu_{1,3}$.[39]

In the gas phase, excitation of ammonia by electron scattering is feasible for energies above 5.14 eV,[40] whereas electron attachment may occur at an energy as low as 4.93 eV.[41] For hot substrate electrons generated by 6.4 eV photons both processes are attainable. For the ammonia/Cu(111) system we also observe photodesorption for excitation with 4.0 eV laser light, albeit with cross sections approximately an order of magnitude smaller than at 6.4 eV. For electron attachment this would imply a downward shift of the gas-phase resonance by at least 1 eV. This can be accounted for by the expected influence of the surface image potential and by the formation of the chemisorption bond. Similar stabilization of a resonance by electronic polarization of the substrate has been proposed to account for photodesorption of molecular oxygen from Pt(111)[36] and Pd(111)[31] for excitation at 3.9 eV and higher energies. Excitation wavelength dependent translational energies have also been reported for photodesorption in the O_2/Pd(111) system. The observed variation in translational energy for different excitation energies was tentatively attributed to the regions with different slopes that are accessible in the excited-state potential when the kinetic energy of the scattering electrons is altered. A more comprehensive explanation of this phenomenon, which we also observed in the ammonia/Cu(111) system, is given by a new approach to electron induced desorption introduced by Harris and Holloway.[42]

B. Isotope effect

The electronic excitation of an adsorbate by electrons or holes is often accompanied by a change of the equilibrium configuration within the adsorption complex. At surfaces most of these electronic excitations are believed to be short-lived with lifetimes ranging from some $\approx 10^{-15}$ to $\approx 10^{-14}$ s.[4] The forces acting along different coordinates of the system during the temporary perturbation induce nuclear motion. The kinetic energy gained can subsequently lead to desorption or dissociation after return to the ground-state potential energy surface. Such a mechanistic picture was developed to account for electron stimulated desorption from surfaces by Menzel, Gomer,[9] and Redhead[10] in 1964 (MGR model). The same year Bardsley *et al.*[43] also developed a rather similar concept to model negative ion formation cross sections for dissociative electron attachment in gas-phase experiments (impulse approximation). Their model was first applied to account for the isotope effect of 200 (!!) in the negative ion formation cross section for dissociative electron attachment at H_2 and D_2.[44] The individual steps of this or the MGR model may be visualized as an initial Franck–Condon transition to an excited-state PES, movement on the excited state PES, relaxation to an eventually desorption or dissociation on the ground-state PES, as illustrated in the left panel of Fig. 12. During the time the system spends in the excited state, a lighter particle will travel further than a heavy one and will thus acquire more kinetic energy. A convenient expression describing this isotope effect, as derived from the above model, is given by[45,46]

$$\frac{\sigma_{m_1}}{\sigma_{m_2}} = \left(\frac{\sigma_{\mathrm{ex}}}{\sigma_{m_1}} \right)^{\sqrt{m_2/m_1}-1} \quad \text{or} \quad \frac{\sigma_{m_1}}{\sigma_{m_2}} = \left(\frac{1}{P_{m_1}} \right)^{\sqrt{m_2/m_1}-1}, \tag{1}$$

where the desorption probability P_{m_1} is connected to the desorption cross section σ_{m_1} by

$$P_{m_1} = \sigma_{m_1}/\sigma_{\mathrm{ex}}.$$

Here σ_{ex} is the excitation cross section which is in general unknown. It should be pointed out that although the basic

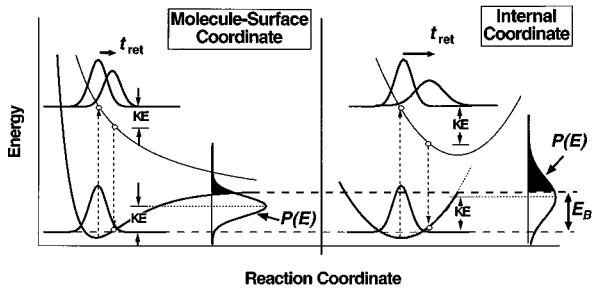

FIG. 12. Schematic illustration of a MGR-type desorption process for two different reaction coordinates in the excited state. Steps leading to desorption are: initial Franck–Condon transition to an excited-state PES; movement on the excited-state PES within the average lifetime τ; quenching at t_{ret} followed by motion on the ground-state PES and eventually desorption if the kinetic energy (KE) exceeds the remaining barrier towards desorption. Two different reaction paths in the excited state are considered: motion along the molecule–surface coordinate (left panel) and motion along an internal coordinate, e.g., the ammonia umbrella mode (right panel).

concept was developed as a one-dimensional model it is also applicable to multidimensional systems as long as the relevant coordinate is associated with the reaction path in the excited state. The experimentally observed isotope effect may then be used to identify this reaction path, i.e., the coordinate in the excited state along which the kinetic energy required to break the molecule–surface bond is gained.

Applying the above formula to the measured isotope effect of 4.1 for photostimulated desorption of NH_3 and ND_3 from Cu(111) (α coverage) with the desorption cross sections σ_{NH_3} and σ_{ND_3} and using the two masses for molecular motion along the molecule–surface coordinate ($m_1=17$, $m_2=20$), we obtain an excitation cross section σ_{ex} of 5.4×10^{-14} cm^2. This cross section of more than 500 Å^2 is physically unreasonable. In other words: the large isotope effect cannot be accounted for by motion along the molecule–surface coordinate in the excited state using reasonable excitation cross sections. In contrast, motion along the inversion coordinate, e.g., with reduced masses 2.5 and 4.2 for NH_3 and ND_3, respectively, would yield a more sensible excitation cross section of 3.2×10^{-19} cm^2. Thus, using the same arguments previously applied to photodesorption of ammonia from GaAs(100) by Zhu *et al.*[6] we also assign the large isotope effect to the fact that the energy required to break the molecule–surface bond stems from nuclear motion in the excited state along an *internal* ammonia coordinate.

Using the MGR model and the above expressions for the isotope effect we may now also try to understand the general trends in the desorption cross sections and resulting isotope effects when the ammonia coverage is altered. Obviously, the probability P_m to overcome the activation energy for desorption (from the ground state) has a crucial influence on the isotope effect. For a given topology of the excited-state PES, the desorption probability depends—if we neglect relaxation phenomena on the ground-state PES—on the excited-state lifetime τ and the ground-state binding energy E_B. Larger binding energies to the substrate require more kinetic energy (in the internal coordinate) to break the bond while shorter lifetimes in the excited state reduce the amount of kinetic energy that can be acquired during the excitation. Both trends lead to a reduced desorption probability. The increase in the isotope effect when going from the high to low coverage phase may thus be attributed to the increasing binding energy E_B ($\approx$0.35 eV β_2 coverage, $\approx$0.48 eV β_1 coverage, and $\approx$0.71 eV α coverage) which reduces the desorption probability.

The energy which is gained by a particle in the excitation–deexcitation cycle is given by a probability distribution $P(E)$, where E is the total—kinetic plus potential—energy. Within the framework of the MGR model this distribution can be calculated using semiclassical Gaussian wave packet dynamics.[47] The corresponding procedure which was developed by Gadzuk results in a Gaussian probability distribution $P(E)$ which is schematically depicted in Fig. 12. However, only a fraction of particles within this probability distribution has acquired enough energy to break the molecule–surface bond, indicated by the shaded areas in the $P(E)$ curves in Fig. 12. This fraction of molecules which can desorb (typically on the order of 10^{-2} to 10^{-4}) depends on the width and position of $P(E)$ with respect to the desorption threshold E_B, i.e., on the total energy gained in the excitation–deexcitation cycle. The mean kinetic energy of desorbed molecules, however, is determined by the shape of the probability distribution above E_B, which is not altered substantially when the center of gravity of $P(E)$ is slightly shifted. Thus, using this model, one does *not* expect a strong correlation between desorption probability and kinetic energy of desorbing particles. This conclusion is in agreement with our observations at $h\nu=6.4$ eV for the mean translational energies at different adsorbate coverages where no pronounced difference in translational energy was found despite the large differences in the desorption yield. It may also account for the similar kinetic energies measured for the two isotopically labeled species despite their different desorption probabilities, which are manifest in the isotope effect. However, using these arguments there is no simple explanation for the strong increase in the isotope effect in the translational energy at 308 nm compared to that at 193 nm.

The observed trends in the isotope effects and desorption cross sections may also be calculated on a semiquantitative level using the so-called displaced oscillator model described by Gadzuk and Holloway.[48] Given that the isotope effect is attributed to intramolecular motion in the excited state, we use this model to calculate the amount of vibrational energy which is acquired by the corresponding ammonia coordinate. When a harmonic oscillator in the ground state is subject to a time-dependent perturbation—representing the forces on the excited-state PES—one may obtain analytical solutions for the population of the nth vibrational level in the coordinate ν after the perturbation is switched off at the time t_{ret}. The individual steps of this MGR-like excitation–deexcitation cycle are basically the same as described above and are displayed in the right panel of Fig. 12. If the force constants in the excited and ground states are the same, one then obtains the simple Poisson distribution for the transition probability $P(0\rightarrow n_\nu)$[48]

$$P_{0\to n_\nu}(t_{\rm ret})=\frac{\beta^{n_\nu}\exp(-\beta)}{n_\nu!}, \tag{2}$$

where β is given by

$$\beta=2\beta_0[1-\cos(\omega t_{\rm ret})] \quad \text{with} \quad \beta_0=\frac{\Delta q^2\cdot\mu}{2\hbar\omega}.$$

Here Δq is the displacement of the two harmonic oscillator potentials, ω is the oscillator frequency in both ground and excited state, $t_{\rm ret}$ the time of return to the ground state, and μ is the reduced mass for motion along that coordinate. It needs to be mentioned that expression (2) is also the exact quantum mechanical excitation probability function.[48]

The condition that ground- and excited-state vibrational frequencies should be identical is well satisfied for the inversion coordinate of gas-phase ammonia,[41] to use this one as an example. To account for the average lifetime τ in the excited state we have furthermore calculated the time weighted average for the transition probability $P(0\to n_\nu)$:

$$P^{\tau}_{0\to n_\nu}=\frac{1}{\tau}\int_0^\infty dt_{\rm ret}\exp\left(-\frac{t_{\rm ret}}{\tau}\right)P_{0\to n_\nu}(t_{\rm ret}).$$

In order to obtain the desired expressions for the coverage depedence of desorption cross sections and isotope effects we then computed the probability of finding a molecule with enough vibrational energy to break the surface bond. For simplicity, this implies that every molecule which is capable of doing so will eventually desorb. This requires that desorption occurs fast with respect to vibrational relaxation, an assumption that seems to be justified for the proposed desorption mechanism (see Sec. V). The desorption probability $P_{\rm des}$ for a given binding energy E_B is then

$$P_{\rm des}(E_B)=\sum_{n_\nu\cdot\hbar\omega\geq E_B}P^{\tau}_{0\to n_\nu}.$$

For the calculation of the isotope effect, $P_{\rm des}(NH_3)/P_{\rm des}(ND_3)$, at arbitrary binding energy we used a linear interpolation between the steps of the energy dependence of $P_{\rm des}(E_B)$. For the low coverage phase α ($E_B=0.71$ eV) we obtained best agreement with the measurement isotope effects of 4.1 for an excited state lifetime τ of 1×10^{15} s. Using this lifetime we then calculated the energy dependence of the desorption probability and isotope effect, see Fig. 13. For the estimated binding energies of the β_1 phase this would yield an isotope effect of 3.1 and for the β_2 phase an isotope effect of 2.4 which is—considering the simplicity of the model—in nice agreement with the experimental trends and isotope effects of 3.4 ± 1.3 and 1.9 ± 0.5, respectively.

This model also accounts— at least qualitatively—for the continuous decrease in the effective cross sections at lower adsorbate coverages as derived from the slope of the yield vs photon exposure curves (Fig. 8). This becomes clear if we keep in mind that strong dipole–dipole interactions in polar adsorption complexes lead to coverage-dependent binding energies, i.e., to coverage-dependent desorption probabilities.

However, a crucial parameter of the whole analysis–namely the excited-state lifetime—remains subject to pure speculation as in most other studies involving such an excitation–deexcitation cycle. This lifetime, which is known to some extend for gas-phase excitations, remains almost completely unknown due to a lack of direct measurements for excitations at surfaces. Theoretical calculations of the $n=1$ and $n=2$ resonance widths Γ for hydrogen in front of an aluminum surface[49] yield approximately 0.3 to 3.0 eV which would correspond to a lifetime of ≈2.0–0.2×10^{-15} s. Keeping in mind that all excited states of free ammonia–which is isoelectronic with neon—and also the first excited states of the anion are associated with promotion of one of the $3a_1$ valence electrons to a Rydberg-like orbital of the molecule,[38] i.e., to a '3*s*', '3*p*'...-like orbital, a comparison with the calculated resonance widths for hydrogen makes the estimated lifetime of 1×10^{-15} s at least plausible.

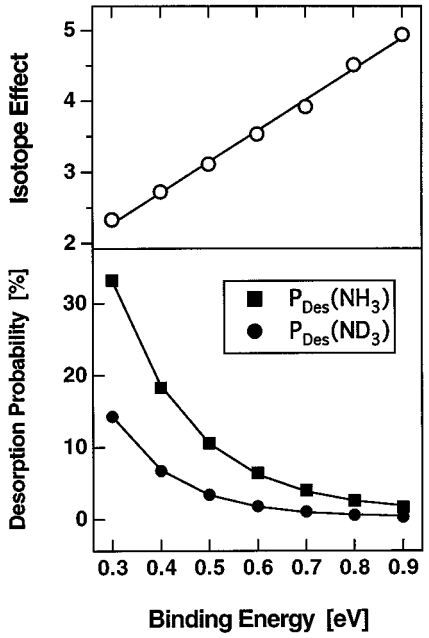

FIG. 13. Calculated dependence of the isotope effect (upper panel) and desorption probability for NH_3 and ND_3, respectively (lower panel) on the adsorbate binding energy (desorption threshold) using the displaced oscillator model described in the text. The results reproduce the observed trend of the coverage dependence for the isotope effect.

To sum up the results of this section: (i) the large isotope effect for the desorption cross sections of NH_3 and ND_3 is attributed to motion along an internal ammonia coordinate in the excited state without assignment to a particular mode at this point; (ii) the trends in the isotope effect and qualitative agreement with the coverage dependence can be attributed to the variation of the desorption probability due to a change in binding energy; (iii) the estimated lifetime of 1×10^{-15} s seems reasonable considering the Rydberg character of the corresponding excited states in gas-phase ammonia.

C. Desorption dynamics

The amount of energy released along the different coordinates of the system during the desorption process provides

an avenue for probing the microscopic forces that are involved in the desorption process. In this section we will discuss what can be learned from the angle-resolved distributions of flux and mean translational energy of desorbed ammonia. In addition we present trajectory calculations on a model PES which are intended to illustrate the proposed coupling mechanism between the ammonia inversion mode and the molecule–surface coordinate. At a semiquantitative level the calculations also yield the energy disposal into translational and vibrational degrees of freedom.

1. Angular-resolved distributions of flux and mean translational energy

As for the ammonia/Cu(111) system, the flux of photodesorbed molecules frequently exhibits angular distributions strongly peaked along the surface normal. This behavior is anticipated for MGR-type reactions in which translational energy is preferentially released along the surface normal. Despite the missing physical background these distributions are commonly characterized by a $\cos^n(\vartheta)$ law angular dependence where ϑ is the polar angle with respect to the surface normal. The flux angular distribution for photodesorption of NH_3 from the high coverage β_2 coverage, depicted in the upper panel of Fig. 10 may best be approximated by a $\cos^{17\pm4}(\vartheta)$ distribution. The wings of the measured distribution, however, deviate significantly from the $\cos^n$ fit. We therefore tried to model these distributions given that translational energy is released exclusively along the surface normal. To calculate the angular distributions of both flux and mean translational energy one then has to evaluate the number density $N(v_x,v_y,v_y)$ for different angles of detection. Given that motions parallel to the surface are independent of the perpendicular one, the number of molecules per unit volume having velocities between v_x, v_x+dv_x, v_y, v_y+dv_y, and v_z, v_z+dv_z may be written as a product of the individual components perpendicular and parallel to the surface[2]:

$$N_v(v_x,v_y,v_z)d^3v = N_{v\parallel}(v_x,v_y)N_{v\perp}(v_z)d^3v.$$

The perpendicular velocity distribution $N_{v\perp}$ is characterized by the mean translational energy $\langle E^{\perp}_{\text{trans}}\rangle$ and the variance $\langle\sigma^2\rangle$—as derived from fitting the measured TOF distributions (for detection along the surface normal). For the velocities parallel to the surface we simply assume that thermal motions prior to excitation are conserved in the desorption process. The distribution $N_{v\parallel}$ is then determined by the sample temperature T_S and frequencies for the frustrated translations. Evaluation of the above expression with $\langle\sigma^2\rangle=0.13$ (the value for a thermal Maxwell–Bolzmann distribution) and conversion to the flux domain then yields the flux angular distribution $f(\vartheta)d\Omega$:

$$f(\vartheta)d\Omega \propto \frac{\cos(\vartheta)d\Omega}{[\sin^2(\vartheta)/T_S + 2k_B\cdot\cos^2(\vartheta)/\langle E^{\perp}_{\text{trans}}\rangle]^2}. \quad (3)$$

Details of the calculation and the more general form for arbitrary $\langle\sigma^2\rangle$ will be presented elsewhere.[50] For the mean translational energy in the flux domain one obtains a similar expression:

$$\frac{\langle E_{\text{trans}}\rangle}{2k_B} = \left(\frac{\sin^2(\vartheta)}{T_S} + \frac{2k_B\cdot\cos^2(\vartheta)}{\langle E^{\perp}_{\text{trans}}\rangle}\right)^{-1}. \quad (4)$$

The distributions resulting from Eqs. (3) and (4) are also depicted in Fig. 10 together with the measured angular distributions using the experimental values for the β_2 coverage $\langle E^{\perp}_{\text{trans}}\rangle=107$ meV and $T_S=90$ K. The excellent agreement of calculated and experimental distributions, also for the mean translational energies, encourages us to attribute the observed angular broadening to thermal motions parallel to the surface prior to the excitation. This implies that during the desorption process no forces are active parallel to the surface (other than thermal excitations) and that kinetic energy from the electronic excitation is transferred essentially into the z coordinate (i.e., along the surface normal).

2. Simulation of desorption dynamics: Trajectory calculations

In the following we discuss the desorption dynamics on the basis of a two-dimensional model which accounts for many of the experimental findings on a semiquantitative level. We first summarize what can be concluded from the above discussion about the relevance of different coordinates for the desorption mechanism: (i) The magnitude of the isotope effect reveals that the energy necessary to break the molecule–surface bond is acquired predominantly by an intramolecular coordinate during a short-lived electronic excitation. (ii) Comparison with the energetically lowest electronic excitations of gas-phase ammonia by either photons or electrons suggests that at the surface the excited state should favor a change from the pyramidal equilibrium geometry towards a more planar configuration.[38] This will result in vibrational excitation of the *inversion mode* (umbrella mode) after deexcitation to the electronic ground state. (iii) The ammonia surface scattering experiments of Kay *et al.*[16] revealed substantial translational to vibrational energy transfer, i.e., a coupling between the inversion mode and the molecule–surface coordinate. The observed coupling should also be operative for chemisorbed ammonia molecules with high vibrational excitation of the inversion mode since the scattering experiments of Kay *et al.* probe similar regions of the ground-state PES above the desorption threshold. During the excitation process other vibrational modes are likely to be excited as well (e.g., the symmetric or asymmetric stretching mode); we believe, however, that coupling of these modes to the desorption coordinate is inefficient when compared to the inversion mode. The desorption mechanism presented below will allow efficient desorption within very few periods of the umbrella vibration. (iv) Angle-resolved flux and translational energy distributions indicate that the excess energy channeled into translation is predominantly released along the surface normal. In view of these observations, we conclude that the simplest description of the desorption process has to include at least the intramolecular umbrella vibration and the motion along the surface normal.

In order to simplify the simulation of desorption dynamics we restrict our model to two dimensions, namely, the molecule–surface coordinate and the inversion mode, where the surface is assumed to be of infinite mass. The inversion

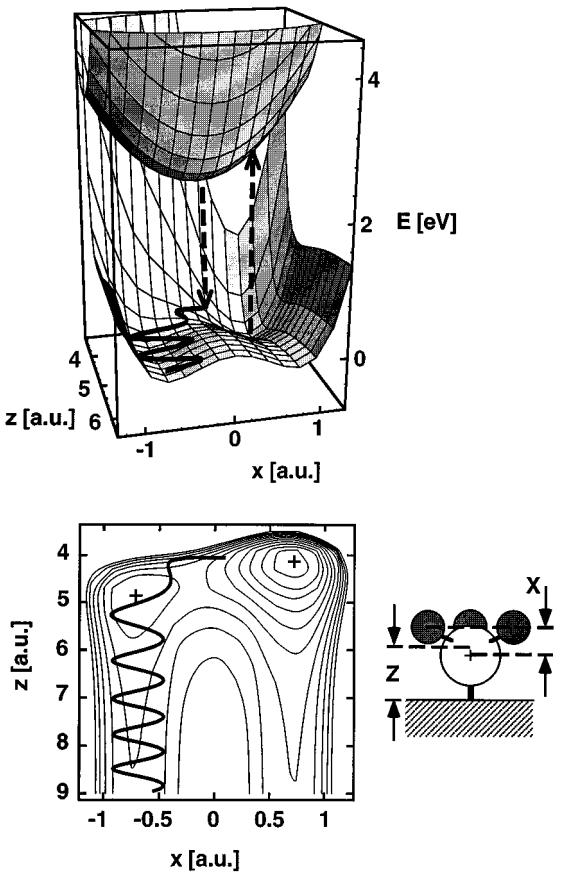

FIG. 14. Model PES of the ground state and excited state, respectively, used in the simulation of the desorption dynamics. The coordinate z refer to the ammonia center of mass to surface distance while x is defined as the distance of the hydrogen plane to the nitrogen atom (see cartoon). The lower section shows a contour plot of the ground-state PES (contour spacing 100 MeV). The solid line displays for a typical desorption event a calculated trajectory which has spent 9 fs on the excited-state PES.

coordinate x is defined by the distance between the plane intersecting the hydrogen nuclei and the nitrogen atom, while the coordinate z refers to the distance of the ammonia center of mass to the surface. The definition of both coordinates is illustrated by the cartoon in Fig. 14.

The desorption process is now modeled on the basis of an MGR-like desorption scheme. The first step involves excitation to an excited-state PES which favors a planar geometry. Movement on this surface transfers potential into kinetic energy in the inversion coordinate. The electronic lifetime in the excited state determines how much of this energy is acquired up to the moment of deexcitation and thereby governs the isotope effect. Movement on the ground-state PES thereafter determines how much energy is eventually channeled into the two degrees of freedom due to coupling of both coordinates.

Some of the general topological aspects of the two-dimensional ground-state PES are inferred from what is known about ammonia in the gas phase and the adsorbed state (theoretical and experimental data). At large distances from the surface the PES will resemble the gas-phase double-well potential with identical minima at $x=\pm 0.72$ a.u. (1 a.u.$=0.529$ Å) which are separated by a barrier of 0.26 eV. Our work function measurements indicate that ammonia is adsorbed with the nitrogen end pointing towards the surface ($x>0$). The depth of the chemisorption minimum is given by the binding energy as derived from our thermal desorption data (0.7 eV, α coverage) while the positions in x and z are adopted from cluster calculations for NH_3 on Cu(100)[32] ($x=+0.7$ a.u., $z=4.1$ a.u.). Its curvature in both coordinates is determined by vibrational frequencies that have been measured for the ammonia/Cu(100) system.[25,33] Furthermore, the electrostatic contribution to the chemisorption bond is expected to be present at arbitrary x due to the strong polar character of the individual nitrogen–hydrogen bonds. This should lead to formation of a second, weaker chemisorption minimum in the inverted geometry ($x<0$) and also to a lowering of the barrier between both minima. The position and depth of the second minimum (depth$=0.2$ eV; $x=-0.72$ a.u., $z=4.8$ a.u.) is guided by the calculations of Burns *et al.* for the NH_3/Pt(111) system. Preliminary results from a calculated PES for the NH_3/Cu system by Saalfrank *et al.* suggest a somewhat larger separation along z between both minima.[51]

For our model calculations we have developed an analytic ground-state potential function which is consistent with the known experimental data and closely follows the topology of the calculated potential energy surfaces as described above. A contour plot is shown in the lower part of Fig. 14. The explicit functional form of the PES is given in the Appendix. Note, that transformation to the ND_3 center of mass leads to a smaller separation, Δz, between the two minima (ND_3: $\Delta z=0.55$ a.u.; NH_3: $\Delta z=0.72$ a.u.). The analytic form of the PES allows us to study the influence of the well depth and position of both minima on the simulation of the desorption dynamics. Trajectory calculations performed on this ground-state PES qualitatively reproduce the vibrational excitation in the inversion mode as observed in the scattering data from Kay *et al.*[16]

Guided by the gas-phase potential of ammonia in the $\tilde{A}$ state, we use a displaced harmonic oscillator potential in both coordinates centered at $x=0$ a.u. and $z=4.1$ a.u. for the excited-state PES. The nitrogen atom is not displaced along the surface normal. The vibrational quantum $\hbar\omega_x=100$ meV along x is chosen close to the gas-phase value, while for $\hbar\omega_z$ we use value for the molecule surface vibration (45 meV for NH_3).[29] Due to the small reduced mass in the internal vibrational coordinate x, motion on this excited-state PES results predominantly in excitation of the inversion mode.

In the ammonia center of mass coordinates the kinetic energy terms in the Hamiltonian separate and the classical two-dimensional Hamiltonian is given by

$$H(x,z,p_x,p_z)=\frac{p_x^2}{2m_x}+\frac{p_z^2}{2m_z}+V(x,z),$$

where p_x and p_z are the linear momenta along x and z and the two coordinates x and z are coupled by the interaction potential $V(x,z)$. The reduced mass in the inversion coordinate m_x is 2.47 (4.2) u, while the total mass is $m_z=17$ (20) u for NH_3 (ND_3), respectively.

The classical equations of motion are

$$\frac{dq}{dt}=\frac{p_q^2}{m_q},$$

$$\frac{dp_q}{dt}=-\frac{\partial V}{\partial q},$$

where q refers to the coordinates x and z, respectively. The calculation follows a procedure developed previously by Hasselbrink.[52] The starting conditions are derived from a random choice of initial coordinates x, z, p_x, and p_z weighted by the appropriate ground-state wave functions.[53] These are approximated by Gaussians determined by the vibrational quanta $\hbar\omega_x=120$ (92) meV and $\hbar\omega_z=45$ (41) meV for NH_3 (ND_3), respectively. We then begin the simulation starting with the initial conditions by integration of the above equations of motion on the excited-state PES (V_{ex}). Quenching of the electronic excitation is modeled by a constant deexcitation probability $P_{dex}=\tau^{-1}$ per unit time for the return to the ground state. This results in an exponentially decaying probability $\exp(-t/\tau)$ for a trajectory to continue on V_{ex} at the time t. If the total energy after deexcitation is above the desorption threshold the trajectory calculation is continued on the ground-state PES.

The simulation revealed two types of desorption events, i.e., trajectories with positive total energy. While approximately 50% ''desorbed'' ($z>10$ a.u.) directly within a few vibrational periods of the inversion mode ($\tau_{vib}\approx 35$ fs) the remainder populated quasibound orbits and did not separate from the surface within several picoseconds, i.e., a time scale longer than what would be inferred from vibrational damping at surfaces.[14,15] Because energy (T_1) relaxation of adsorbate vibrations on metals is known to be fast due to damping by electron-hole pair excitations, only those desorption events were considered for which the trajectory left the coupling regime within the first several hundred femtoseconds after deexcitation. To exclude physically unlikely desorption events from the calculations, we terminated integration of trajectories at 1.2 ps. The influence this had on our results was negligible (within changes of a few percent for the isotope effect) when this time limit was altered from 1 to 1.5 ps.

The average lifetime in the excited state was adjusted to $\tau=1.1$ fs to yield reasonable desorption probabilities of the order of 10^{-3} and good agreement with the measured isotope effect for the α coverage. Note that trajectories which actually desorb spend a much longer time (typically 5–8 fs) on V_{ex}. Calculation of 2×10^6 and 4×10^6 trajectories for NH_3 and ND_3, respectively, rendered a desorption probability of $P_{d,NH_3}=0.18\%$ and $P_{d,ND_3}=0.045\%$ which corresponds to an isotope effect of $\sigma_{NH_3}/\sigma_{ND_3}=4.2$. Our calculations indicate that the isotope effect is mainly determined by the lifetime τ in the excited state and that possible contributions from the ground-state PES, e.g., due to different coupling efficiencies for both isotopes are negligible.

The calculated translational and vibrational energy distributions of the desorbing molecules are displayed in Fig. 15. An average translational energy of $\langle E_{trans,\,NH_3}\rangle = 108$ meV and $\langle E_{trans,\,ND_3}\rangle = 90$ meV is obtained for NH_3 and

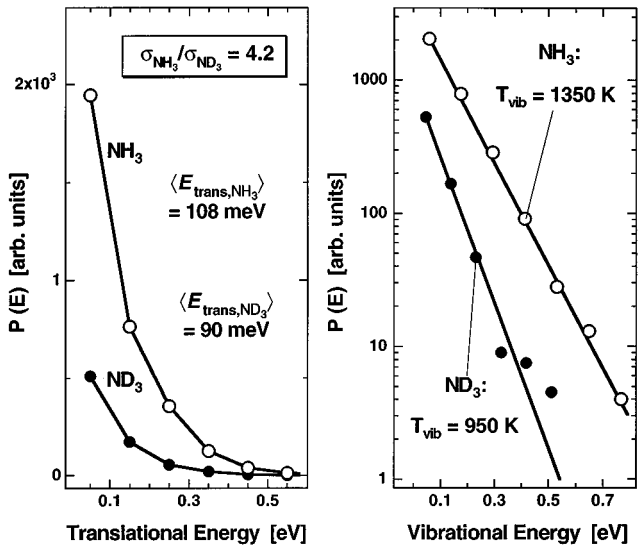

FIG. 15. Calculated energy release into the translational and vibrational degrees of freedom obtained from trajectory calculations (see the text). Left graph: desorption probability vs translational energy for NH_3 and ND_3. Right graph: semilogarithmic plot for the vibrational population of desorbed NH_3 and ND_3.

ND_3, respectively. These numbers are in fair agreement with our experimental data [$\langle E_{trans}\rangle=102$ (93) meV for NH_3 (ND_3)] for ammonia on Cu(111). The model also yields an isotope effect for the mean vibrational energy [$\langle E_{vib}\rangle=115$ (80) meV for NH_3 (ND_3)]. These isotope effects in the average vibrational and translational energies, which are small compared with the isotope effects in the yield, can be rationalized if one considers that a heavier isotope acquires on the average less energy in the excited state and hence less energy will be available after deexcitation to be channeled into the different degrees of freedom. From the trajectory calculations we find no indication for a correlation between the translational and vibrational energy of desorbed ammonia.

The calculated energy release into vibrational excitation of the desorbed molecules may be compared with recent quantum-state-resolved data for stimulated desorption of ammonia. When ammonia was desorbed by electron impact from Pt(111) Burns *et al.*[12] report vibrational temperatures of about 950 K ($\langle E_{vib}\rangle\approx 85$ meV), identical for both isotopes within the error bars. Comparison with their experiments shows that the energy disposal, particularly in the inversion mode of the desorbing ammonia, is overestimated by our model calculation. This may be attributed to the low dimensionality of our model which prevents energy release into other modes. Particularly, one might expect a coupling between the inversion coordinate and the rotational degrees of freedom as suggested by Burns *et al.* Furthermore, the surface has been treated as rigid and electronic damping of adsorbate vibrations in the electronic ground state was completely neglected for the first 1.2 ps. Even with these simplifying approximations, our model is consistent with many of the experimental findings, at least on a semiquantitative level.

Further analysis of our trajectory calculations indicates

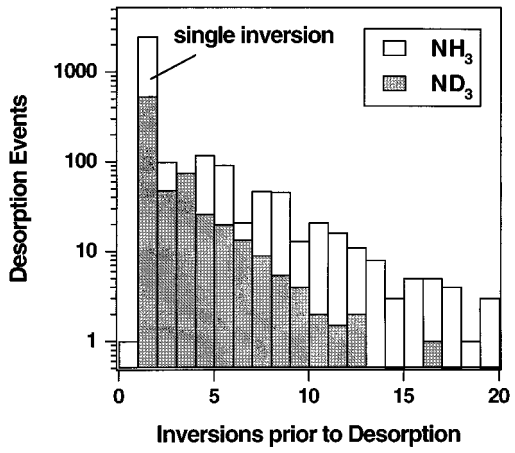

FIG. 16. Number of desorption events vs number of inversions performed prior to desorption as derived from the trajectory calculations. Within the first picosecond the majority of all desorption events (82%) follows a direct reaction path and performs a single inversion only.

that ammonia molecules leave the surface exclusively in an inverted geometry ($x<0$), i.e., with the hydrogen atoms pointing towards the surface. A trajectory representing a typical desorption event is shown in Fig. 14. After energy has been acquired by the inversion coordinate during the excitation–deexcitation cycle the molecule undergoes an *inversion on the ground-state* PES. Obviously, desorption occurs rapidly on a time scale comparable to the intramolecular vibrational period ($\tau_{\mathrm{vib}}\approx 35$ fs). This reinforces our assumption that damping on the ground-state PES can be neglected.

We find that within the first picosecond the majority (82%) of all desorption events is due to such rapid and direct desorption processes while a small fraction (18%) performs a few oscillations between both minima of the ground-state PES prior to desorption. This is illustrated in the histogram shown in Fig. 16. Those desorption events that have undergone multiple inversions prior to desorption (a process which might be termed ''vibrational predesorption'') may contribute more strongly to the desorption yield provided that the relaxation time of the inversion mode exceeds several vibrational periods. If the displacement between the two minima of the ground-state PES is increased we find that the relative contribution of this second channel also increases. However, the general results of our model, i.e., the large isotope effect and the comparable amount of energy disposed into translation and vibration, are unaffected by such details of the PES.

An interesting aspect of the desorption path seems to be its resemblance to the reaction paths frequently found for elbow-type potentials in the case of a so-called ''early barrier,'' e.g., in gas-phase $A-BC$ exchange reactions.[54] In this picture the vibrational energy initially acquired in the inversion coordinate x adiabatically ends up in translational energy along z.[55] The coupling on the PES, which is related to the curvature along the reaction path, determines the energy interchange between the two degrees of freedom. In summary we conclude that the isotope effect is determined by the properties of the excited-state PES (e.g., the lifetime, slope, etc.) while the energy partitioning between the internal and translational coordinates is related to the details of the coupling on the ground-state PES.

V. SUMMARY

The UV stimulated photodesorption for the ammonia/Cu(111) system has been investigated at three coverages in the submonolayer regime. From our results we conclude that the desorption process involves the following steps:

(1) At both laser wavelengths used (193 and 308 nm) light absorption in the substrate leading to generation of hot electron-hole cascades is believed to be the primary excitation step leading to desorption. Temporary localization of the excitation at the adsorbate is then assumed to occur via electron scattering from ammonia molecules.

(2) The measured isotope effect in the photodesorption cross section of NH_3 and ND_3, respectively, is attributed to the fact that the energy necessary to break the molecule–surface bond is acquired by an internal coordinate of the molecule. The observed variation in the isotope effect with adsorbate coverage is attributed to changes in the adsorbate binding energy and can be calculated on the basis of a simple excitation–deexcitation MGR-like desorption mechanism when we employ an excited-state lifetime of 1×10^{-15} s.

(3) Angle-resolved distributions of flux and mean translational energy indicate that energy release into translation occurs predominantly along the surface normal. The angular width can be assigned to molecular motions parallel to the surface prior to excitation.

(4) Energy interchange between an internal ammonia mode and the molecule–surface coordinate requires coupling of both coordinates. Our trajectory calculations indicate that the inversion mode is particularly promising to account for efficient coupling. Ammonia is predicted to desorb rapidly within a few vibrational periods in an inverted geometry, i.e., with the hydrogen atoms pointing towards the surface. Energy disposal into translational and vibrational degrees of freedom is not correlated and is found to be of similar magnitude.

To improve our understanding of the desorption mechanism, state-resolved detection including also a characterization of other than the umbrella mode would be beneficial.

ACKNOWLEDGMENTS

We wish to thank Eckart Hasselbrink, Kurt Kolasinski, and Winfried Nessler for many helpful and profitable discussions during the course of this work. Special thanks to Eckart Hasselbrink who kindly provided us his program for trajectory calculations.

APPENDIX

In the following we give the analytic form of the ground PES used in the trajectory calculations (see Sec. V B). The coordinate r is defined as the distance between the surface and the nitrogen atom and the coordinate x is defined by the distance between the plane intersecting the hydrogen nuclei and the nitrogen atom, respectively. Transformation into the

ammonia center of mass coordinates z, x is straightforward. All numbers and variables are in atomic units.

The ground-state potential $V_g(x,r)$ is modeled by a modified Morse potential plus a term approximating the gas-phase double-well potential along x:

$$V(x,r)=E(x)\left\{\left[1-\exp\left(-\delta\left\{r-r_0 - 1.07\ \sin^2\left[\frac{\pi}{5}\left(x/x_0-\frac{3}{4}\right)\right]\right\}\right)\right]^2-1\right\} + D_x(0.44x^4-0.46x^2+0.12)$$

with

$$E(x)=E_B\left\{0.3+0.7\ \cos^2\left[\frac{\pi}{4}\,(x/x_0-1)\right]\right\}$$

and

$$\delta=\sqrt{\frac{m_z\omega_z^2}{2E_B}}.$$

Here, $D_x=m_x\cdot\omega_x^2$, E_B is the binding energy for chemisorption, ω_z and ω_x are the vibrational quanta, and $r_0=4.0$ a.u. and $x_0=0.7$ a.u. are the equilibrium distances along r and x, respectively ($\hbar\omega_z=45$ meV and $\hbar\omega_x=120$ meV for NH_3, $E_B=0.7$ eV). The mass m_z is the total ammonia mass and m_x is the reduced mass along x.

The surface to nitrogen atom distance r transforms into the ammonia center of mass coordinate z according to $r=z-x\cdot m_3/m_z$, where m_3 is the mass of the three hydrogen or deuterium atoms, respectively.

[1] W. Ho, Surf. Sci. **299/300**, 996 (1994).
[2] E. Hasselbrink, in *Laser Spectroscopy and Photochemistry on Metal Surfaces*, edited by H. L. Dai and W. Ho (World Scientific, Singapore, in press).
[3] R. E. Palmer and P. J. Rous, Rev. Mod. Phys. **64**, 383 (1992).
[4] P. Avouris and R. E. Walkup, Annu. Rev. Phys. Chem. **40**, 173 (1989).
[5] I. Hussla, H. Seki, T. J. Chuang, Z. W. Gortel, H. J. Kreuzer, and P. Piercy, Phys. Rev. B **32**, 3489 (1985).
[6] X.-Y. Zhu and J. M. White, Phys. Rev. Lett. **68**, 3359 (1992).
[7] X.-Y. Zhu, M. Wolf, T. Huett, and J. M. White, J. Chem. Phys. **97**, 5856 (1992).
[8] X.-Y. Zhu, M. Wolf, T. Huett, and J. M. White, J. Chem. Phys. **97**, 5868 (1992).
[9] D. Menzel and R. Gomer, J. Chem. Phys. **41**, 3311 (1964).
[10] P. A. Redhead, Can. J. Phys. **42**, 886 (1964).
[11] X.-Y. Zhu, J. Chem. Phys. **98**, 3410 (1993).
[12] A. R. Burns, D. R. Jennison, E. B. Stechel, and Y. S. Li, Phys. Rev. Lett. **72**, 3895 (1994).
[13] A. R. Burns, E. B. Stechel, and D. R. Jennison, J. Chem. Phys. **101**, 6318 (1994).
[14] M. Head-Gordon and J. C. Tully, J. Chem. Phys. **96**, 3939 (1992).
[15] M. Morin, N. J. Levinos, and A. L. Harris, J. Chem. Phys. **96**, 3950 (1992).
[16] B. D. Kay, T. D. Raymond, and M. E. Coltrin, Phys. Rev. Lett. **59**, 2792 (1987).
[17] R. S. Mackay, K. H. Junker, and J. M. White, J. Vac. Sci. Technol. A **12**, 2293 (1994).
[18] H. C. Chang and G. E. Ewing, Phys. Rev. Lett. **65**, 2125 (1990).
[19] D. Burgess, Jr., P. C. Stair, and E. Wietz, J. Vac. Sci. Technol. A **4**, 1362 (1986).
[20] H. Behrens and G. Ebel, in *Physik Daten* (Fachinformationszentrum, Karlsruhe, 1981), p. 34.
[21] F. Budde, T. Gritsch, A. Mödl, T. J. Chuang, and G. Ertl, Surf. Sci. **178**, 798 (1986).
[22] T. Hertel, E. Knoesel, E. Hasselbrink, M. Wolf, and G. Ertl, Surf. Sci. **317**, L1147 (1994).
[23] W. Steinmann, J. Appl. Phys. A **49**, 365 (1989).
[24] G. Kubiak, Surf. Sci. **201**, L475 (1988).
[25] K. J. Wu and S. D. Kevan, J. Chem. Phys. **94**, 7494 (1991).
[26] G. B. Fisher, Chem. Phys. Lett. **79**, 452 (1981).
[27] C. Benndorf and T. E. Madey, Surf. Sci. **135**, 164 (1983).
[28] P. S. Bagus and K. Hermann, J. Chem. Phys. **81**, 1966 (1984).
[29] W. Biemolt, G. J. C. S. v. d. Kerkhof, P. R. Davies, A. P. J. Jansen, and R. A. Santen, Chem. Phys. Lett. **188**, 477 (1991).
[30] E. Hasselbrink, S. Jakubith, S. Nettesheim, M. Wolf, A. Cassuto, and G. Ertl, J. Chem. Phys. **92**, 3154 (1989).
[31] F. Weik, A. d. Meijere, and E. Hasselbrink, J. Chem. Phys. **99**, 682 (1993).
[32] L. G. M. Pettersson and J. C. W. Bauschlichter, J. Vac. Sci. Technol. A **4**, 1470 (1985).
[33] P. R. Davies and M. W. Roberts, J. Chem. Soc. Faraday Discuss. 2 **88**, 361 (1992).
[34] L. J. Richter, S. A. Buntin, D. S. King, and R. R. Cavanagh, Phys. Rev. Lett. **186**, 427 (1991).
[35] X.-L. Zhou, X.-Y. Zhu, and J. M. White, Surf. Sci. Rep. **13**, 73 (1991).
[36] I. Harrison, V. A. Ukraintsev, and A. N. Artsyukovich, SPIE Proc. **2125** (in press).
[37] W. D. Mieher and W. Ho, J. Chem. Phys. **99**, 9279 (1993).
[38] M. N. R. Ashfold, C. L. Bennett, and R. J. Stickland, Comments At. Mol. Phys. **19**, 181 (1987).
[39] M. B. Arfa, F. Edard, and M. Tronc, Chem. Phys. Lett. **167**, 602 (1990).
[40] S. Cvejanović, J. Jureta, M. Minić, and D. Cvejanović, J. Phys. B. **25**, 4337 (1992).
[41] K. L. Stricklett and P. D. Burrow, J. Phys. B **19**, 4241 (1986).
[42] S. Harris, S. Holloway, and E. Hasselbrink, Nucl Instr. Meth. (in press).
[43] J. N. Bardsley, A. Herzenberg, and F. Mandl, in *Atomic Collision Processes*, edited by M. R. C. McDowell (North-Holland, Amsterdam, 1964), p. 415.
[44] G. J. Schulz and R. K. Asund, Phys. Rev. **158**, 25 (1967).
[45] R. D. Ramsier and J. J. T. Yates, Surf. Sci. Rep. **12**, 243 (1991).
[46] M. Wolf, S. Nettesheim, J. M. White, E. Hasselbrink, and G. Ertl, J. Chem. Phys. **94**, 4609 (1991).
[47] J. W. Gadzuk and C. W. Clark, J. Chem. Phys. **91**, 3174 (1989).
[48] J. W. Gadzuk and S. Holloway, Progr. Surf. Sci. **26**, 87 (1987).
[49] P. Nordlander and J. C. Tully, Phys. Rev. Lett. **61**, 990 (1988).
[50] T. Hertel, M. Wolf, and G. Ertl (in preparation).
[51] P. Saalfrank and J. Manz (private communication).
[52] E. Hasselbrink, Chem. Phys. Lett. **170**, 329 (1990).
[53] R. Schinke, J. Chem. Phys. **92**, 3195 (1988).
[54] J. C. Polanyi and W. H. Wong, J. Chem. Phys. **51**, 1439 (1969).
[55] S. Holloway and G. R. Darling, Comments At. Mol. Phys. **27**, 335 (1992).